IEEE Photonics Journal
An IEEE Photonics Society Publication

# Design and Demonstration of Apodized Comb Filters on SOI

Volume 4, Number 4, August 2012

Venkat Veerasubramanian
Guillaume Beaudin
Alexandre Giguere
Boris Le Drogoff
Vincent Aimez
Andrew G. Kirk

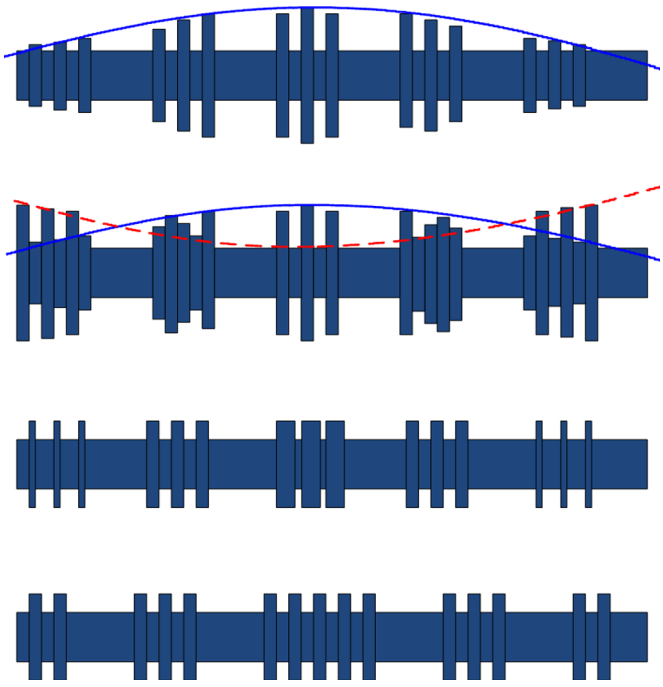

DOI: 10.1109/JPHOT.2012.2204971
1943-0655/$31.00 ©2012 IEEE

# Design and Demonstration of Apodized Comb Filters on SOI

**Venkat Veerasubramanian,[1] Guillaume Beaudin,[2] Alexandre Giguere,[2] Boris Le Drogoff,[3] Vincent Aimez,[2] and Andrew G. Kirk[1]**

[1]Department of Electrical and Computer Engineering, McGill University, Montreal, QC H3A 2A7, Canada
[2]Department of Electrical and Computer Engineering, University of Sherbrooke, Sherbrooke, QC J1K 2R1, Canada
[3]INRS-EMT, Varennes, QC J3X 1S2, Canada

*DOI: 10.1109/JPHOT.2012.2204971*


Manuscript received May 4, 2012; revised June 12, 2012; accepted June 13, 2012. Date of publication June 15, 2012; date of current version July 2, 2012. Corresponding author: V. Veerasubramanian (e-mail: venkat.veerasubramanian@mail.mcgill.ca).

**Abstract:** We report on the design, modeling, and characterization of apodized comb filters in the silicon-on-insulator platform. These devices are based on sampled gratings, wherein the comb response is generated by a convolution of a regular grating by a predetermined periodic sampling function. We show that dual and complementary apodization of the etch depth in the marks and spaces ensures a near-zero dc index change over the length of the device and avoids the unwanted sidelobes obtained in a single apodized device. Comb filters with a 40-dB side-mode suppression ratio, a 92-GHz clear bandwidth, 200-GHz channel spacing, and a 120-dB/dec rolloff have been theoretically proposed. An experimental demonstration of the fabricated devices is also presented, and the performance is compared with the numerical simulations.

**Index Terms:** Waveguide devices, optical filters, Bragg gratings, apodization.

## 1. Introduction

Fast tunable filters are necessary in DWDM networks for robust wavelength filtering as well as packet switching over a range of wavelengths [1]. Multichannel tunable comb filters are a suitable candidate for on-the-fly switching of a range of wavelength channels along the ITU-T grid [2], [3]. While ring-resonator-based devices have a good tuning range, they have limited bandwidth and extinction due to their Lorentzian response. Ideally, the generated combs need to be spectrally flat, with fixed channel spacing, and bandwidth occupying at least 50% of the channel spacing. While ultrawide frequency combs have been generated for applications in precision metrology using nonlinear effects in resonant microcavities [4], biosensing and molecular fingerprinting [5], and in spectroscopy [6], these approaches cannot be used to create combs for wavelength filtering due to their relatively narrow bandwidths in the channels. Hence, spectral response and dispersion-engineered gratings have been used for this purpose. In this article, we propose a design for apodized comb filters based on sampled gratings with 100- and 50-GHz channel spacing on silicon-on-insulator (SOI). Two of these sampled gratings can be used back-to-back to effectively create a high side-mode suppression ratio (SMSR) optical filter employing the Vernier effect [7]. Apodized filters have been demonstrated in fibers and III–V material systems by modulating the refractive index along the grating region using appropriate taper functions [8], [9]. We propose a dual

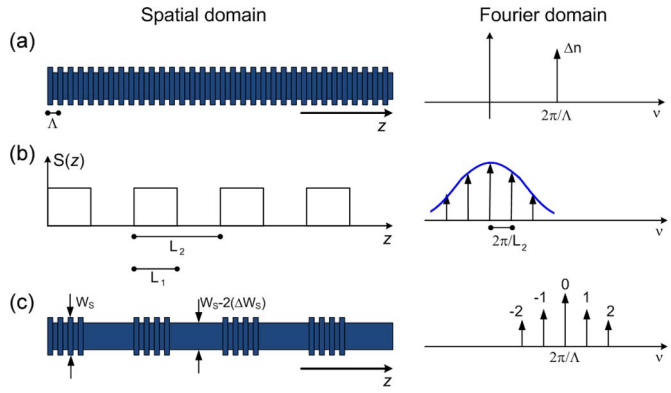


Fig. 1. Top view of the real space and Fourier domain representation of (a) the grating, (b) the sampling function $S(z)$, and (c) the convolution of the two functions resulting in the components of the sampled grating.

complementary tapering of the etch depths in the marks and spaces in the gratings as a means to avoid the sharp residual resonances observed at shorter wavelengths around the Bragg resonance peak in nonuniform gratings. This effect is more pronounced in high-index-contrast gratings. We also demonstrate combs with SMSR $>$ 40 dB, and low and linear chromatic dispersion within the channel. Laterally coupled vertical sidewalled gratings have been employed in our designs, since they have the advantage of a single-step fabrication of the waveguide as well as the grating structure [10], whereas surface corrugations require an additional lithographic step [11]. In addition, surface corrugations are much harder to apodize in terms of varying the etch depth in a modulated fashion along the device, whereas sidewalled gratings offer us the advantage of effective side etch depth modulation easily [12], thereby creating a good apodization profile.

## 2. Design and Analysis

Sampled gratings consist of a regular grating convoluted at appropriate intervals using a sampling function. The periodic modulation of the gratings leads to a reflection spectrum with periodic maxima and a *sinc* function envelope. It is well known that the grating reflectivity spectrum has contributions from the spatial distribution of the actual structure [13]. The Fourier components of the sampled grating are obtained by convolving the components of the transform of a single grating with that of the sampling function as shown in Fig. 1. It is shown that this leads to a comb of wavelength components with a fixed channel separation around the Bragg wavelength. Assuming the grating coupling coefficient of the regular grating is $\kappa_0$, the coupling coefficient of the $n$th Fourier component of the sampled grating is given by [14]

$$\kappa(n) = \kappa_0 \frac{L_1}{L_2} \frac{\sin(\pi n L_1/L_2)}{\pi n L_1/L_2} e^{-i\pi n L_1/L_2}. \tag{1}$$

The reflectivity profile of the sampled grating can be obtained using coupled-mode theory as

$$r(\lambda) = \sum_n \frac{i\kappa^*(n)\sin(\gamma(n)L)}{\gamma(n)\cos(\gamma(n)L) - i\Delta\beta(n)\sin(\gamma(n)L)} \tag{2}$$

where the detuning from the $n$th order is given by

$$\Delta\beta(n) = \frac{2\pi n_{\text{eff}}(\lambda)}{\lambda} - \frac{\pi}{\Lambda} - \frac{\pi n}{L_2} \tag{3}$$

$$\gamma(n) = \sqrt{\Delta\beta(n)^2 - \kappa(n)^2}. \tag{4}$$

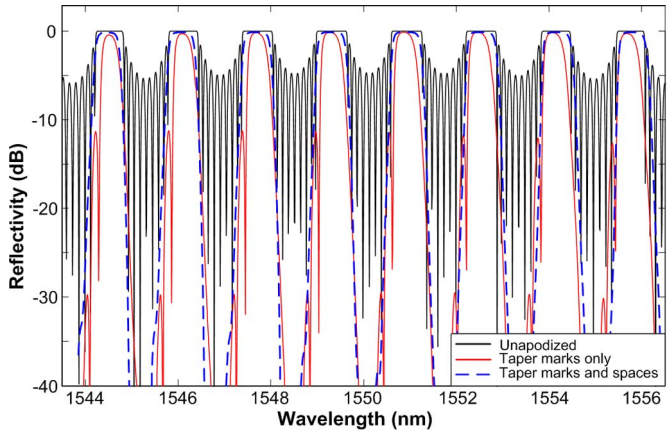


Fig. 2. Reflectivity of an unapodized comb filter (Black solid), apodized using the scheme in Fig. 3(a) (Red solid), and apodized using the scheme in Fig. 3(b) (Blue dash).

Here, $L$ is the length of the sampled grating, $\Lambda$ is the grating period, and $n_{\text{eff}}$ is the group index. The waveguide width $W_S$ and the sidewall etch depth $\Delta W_S$ are as indicated in Fig. 1. Neglecting waveguide losses, the peak reflectivity of the sampled grating at the Bragg wavelength $\lambda_B$ is given by $R_{\text{max}} = \tanh^2(\kappa_0 L)$, whereas the spacing between the channels or the reflectivity peaks is $\Delta\lambda = \lambda_B^2/2n_{\text{eff}}L_2$. Hence, a specific channel spacing $\Delta\lambda$ can be achieved by varying $L_2$. The reflectivity profile of an unapodized sampled grating is shown in Fig. 2. The results were computed using eq. (2) and verified using a transfer-matrix method based on the coupled-mode theory [15]. The SOI wafer is assumed to have a device layer of 260 nm, the waveguide width $(W_S)$ is 1 $\mu$m, side etch depth $(\Delta W_S)$ of 75 nm, and period $\Lambda = 272$ nm. The sampling period $L_1 = 13.2$ $\mu$m, the sampling ratio defined as $L_2/L_1$ is 20, and the number of samples is 10, leading to a total device length of 2.62 mm. The numerical and experimental results presented are all for TE polarization. It is seen that the peak reflectivity is close to unity, whereas the side-mode suppression ratio is less than 3 dB. Such high sidelobe levels make them unsuitable as filters.

When the grating coupling coefficient $\kappa$ is modulated such that it is maximum at the center of the grating and lower toward the edge, the SMSR can be drastically increased [16]. This can be achieved in several ways as indicated in Fig. 3: by modulating the duty cycle of the gratings, by modulating $L_1$ to be maximum at the center, or by modulating the sidewall etch depth. Thus, sidewalled gratings offer us an advantage over conventional surface corrugations in terms of apodization, wherein $\kappa$ can be modulated by modulating $\Delta W_S$. It is also important to keep the effective refractive index in the marks and spaces (we refer to the unetched and etched regions in the waveguide grating as marks and spaces, respectively) constant along the length of the device in order to avoid an undesirable chirp. Several windowing functions (Hamming, Blackman, raised cosine, and Kaiser) have been proposed for effective tapering of the coupling coefficient [17]. Fig. 3(a) shows the top view of the proposed device, wherein the waveguide width in the marks in the grating region is modulated using the raised cosine function

$$\Delta W_S = \Delta W_{S,\text{max}} \sin^2(\pi z/L). \tag{5}$$

Fig. 3(b) shows the proposed dual tapering scheme, where the widths of the marks and spaces are tapered using complementary functions, so that the average spatial index along the device is almost constant (i.e., zero dc index change). The other scheme involving tapering the duty cycle of the gratings is fabrication limited due to the small mark widths in the edges of the device, as shown in Fig. 3(c). Fig. 2 shows the reflectivity spectrum of the regular and apodized comb filters around 1550 nm. A comb with a 1.6-nm channel separation and a 0.8-nm clear bandwidth is obtained. The various device dimensions are as indicated earlier. Fig. 4(a) shows the reflectivity profiles of the central channel of devices with apodization profiles as indicated in Fig. 3(a) and (b), respectively.

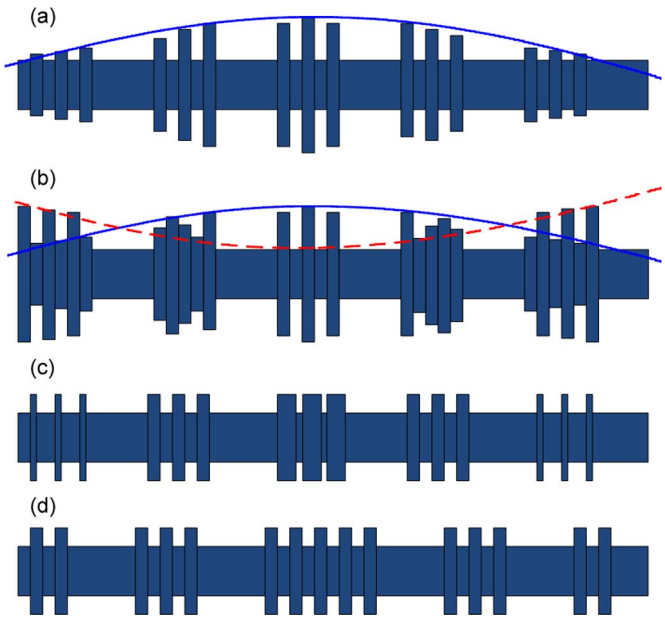


Fig. 3. Top view indicating various apodization schemes: (a) modulating the finger width in the marks alone; (b) modulating the finger width in marks and spaces, the blue and red curves represent the envelope of the tapering function in the marks and spaces, respectively; (c) modulating the duty cycle; and (d) modulating $L_1$ or the number of periods in each pitch.

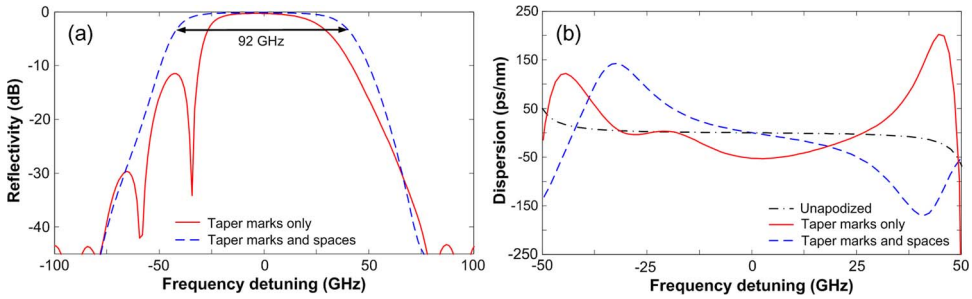


Fig. 4. (a) Response of the central channel. The red curve shows an apodized grating with undesired sidelobes (nonzero dc index), whereas the blue dashed curve shows an apodized grating (near-zero dc index) with > 40 dB SMSR and good symmetry around the Bragg wavelength. (b) Chromatic dispersion within the clear bandwidth for various designs.

It is clearly seen that sidelobes are still present at the shorter wavelengths in the device with a nonzero dc index (average spatial index) change, as previously observed in fiber Bragg gratings [18]. This is because the wings of the grating act as a parasitic Fabry–Perot cavity at shorter wavelengths [19]. If the dc index change is made to be zero, i.e., the average effective index in the marks and spaces is constant along the length of the grating, as in the design in Fig. 3(b), the reflection spectrum becomes symmetric. It is seen that effective apodization provides an almost top-hat filter spectrum with a 40-dB rejection ratio, a 3-dB bandwidth of 92 GHz, and a very steep rolloff of 120 dB/dec. The computed chromatic dispersion within the clear bandwidth of the central channel is shown in Fig. 4(b). It is seen that dispersion is linear in the center of the channel in the dual apodized device, whereas it displays nonlinear distortion in the single apodized device. The residual dispersion can be compensated using a prechirped grating section [20]. Fig. 5 shows the response of a DWDM filter with 0.8-nm channel spacing and a 46-GHz bandwidth, with an SMSR of 40 dB. The grating $L_1 = 26.42$ $\mu$m and the other dimensions are as for the 1.6-nm channel-spaced design.

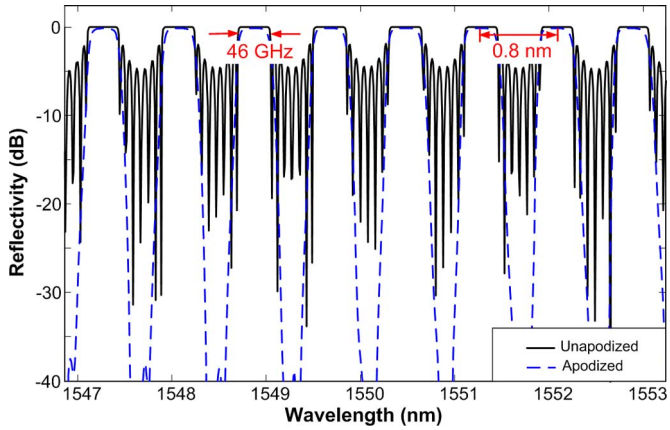


Fig. 5. Filter response of a comb filter with 0.8-nm DWDM channel spacing and 50-GHz bandwidth.

These optical comb filters can be used for switching a range of channels by refractive index modulation of silicon either by plasma dispersion due to carrier injection or by thermal modulation. The change in the refractive index and the electro-absorption coefficient due to carrier injection in silicon at 1.55 $\mu$m can be found in [21]. Numerical simulations using the transfer-matrix method show that a refractive index change of $10^{-3}$ is necessary for shifting the combs (from transmission to reflection) by 0.4 nm in a 0.8-nm spaced comb. This index change of $10^{-3}$ corresponds to a change in the electron density of $2 \times 10^{17}$ cm$^{-3}$ and is within achievable experimental limits [22]. On the other hand, the thermo-optic coefficient of silicon is given by dn/dT $= 1.86 \times 10^{-4}/^{\circ}$C [23]. This indicates that an index change of $10^{-3}$ can also be achieved by effectively raising the temperature along the device in a controlled environment by about 6 $^{\circ}$C.

## 3. Fabrication and Experimental Analysis

The comb filters presented here were fabricated on a SOI substrate with a 260-nm silicon device layer and a 2-$\mu$m buried oxide layer. The devices were patterned by e-beam lithography at 100 keV with a Vistec VB6 UHR-EWF beamwriter on samples spin coated with 140 nm of ZEP520A electron-beam resist. A beam deflection field size of 100 $\mu$m $\times$ 100 $\mu$m was used in order to reduce the stitching errors below 5 nm. After the exposure, the resist patterns were transferred to silicon by using an inductively coupled plasma (ICP) etch recipe with $SF_6/C_4F_8$ chemistry. The Surface Technology Systems (STS) reactor used had a power of 600 W to the coil and 10 W to the platen. The silicon layer was etched all the way to the buried oxide layer. Samples were then cleaned, 200 nm of PMMA electron-beam resist was spin coated, and grating couplers (for coupling light from optical fibers) were patterned by e-beam lithography at 20 keV with a modified LEO 1530 SEM (field size of 20 $\mu$m $\times$ 20 $\mu$m). Grating couplers with a 120-nm etch depth were then obtained using the same ICP etching recipe as above. Fig. 6(a)–(c) shows SEM images of the fabricated devices (after the silicon etch step and resist removal) indicating the tapering of the etch depth along the device. These samples show effective tapering from 220 nm down to 52 nm in the marks along the length of the device. Fig. 6(d) shows a tilt view of a section of the device indicating the measured grating period of 270 nm. This also illustrates the smooth sidewalls and the near-rectangular profile of the gratings, indicative of the high fabrication quality of our devices.

The measured waveguide widths as well as the period of the gratings (270 nm) had deviations of only $\pm$5 nm compared with the target values. However, an underestimated exposure bias induced a deviation of approximately 11 nm in the space dimensions, leading to a measured duty cycle in the fabricated devices of approximately 42%, whereas the numerical results presented were for devices assuming a duty cycle of 50%. This reduction in the duty cycle reduces the channel bandwidth from 0.8 to 0.6 nm. However, this does not affect the channel spacing, which primarily depends on the sampling frequency of the gratings.

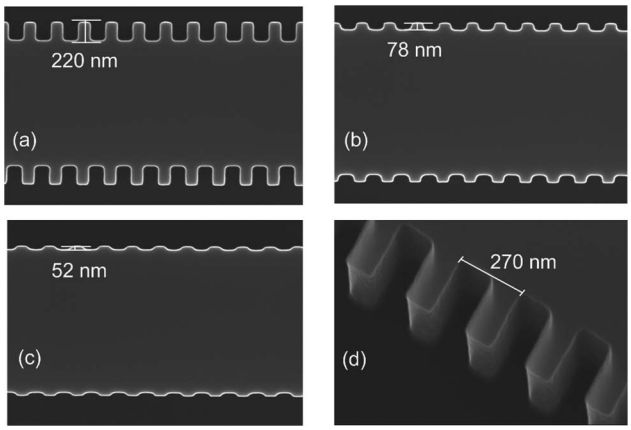


Fig. 6. (a)–(c) SEM micrographs of various sections along the sampled grating indicating etch depths ranging from 220 nm down to 52 nm. (d) A 30° tilt view of the gratings illustrating the smooth sidewalls and the rectangular profile of the etched gratings.

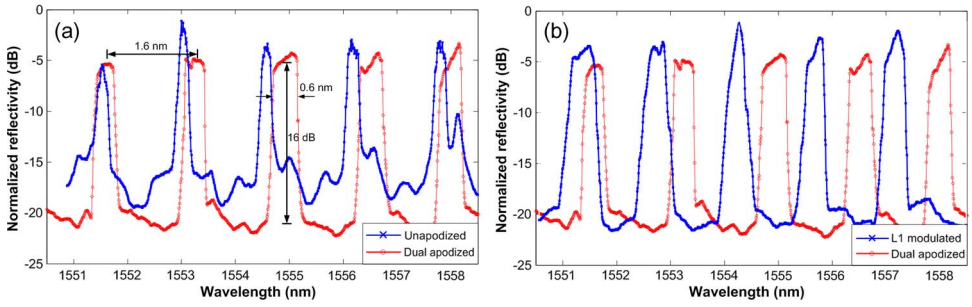


Fig. 7. (a) Measured reflectivity in the dual apodized and unapodized devices. The apodized devices showed a 16-dB SMSR, with 1.6-nm comb spacing, and a 0.6-nm 3-dB bandwidth in the central channel. (b) Comparison of the reflection spectra of the devices with dual apodization and where $L_1$ has been modulated as indicated in Fig. 3(d).

The fabricated devices were tested using a vertical coupling setup for routing light in and out of the chip. Cleaved SMF-28 fibers aligned at 6° to the vertical were precisely manipulated using nano-positioning stages at both the input and output ends. Custom fiber chucks were used to hold the fibers vertically. A broadband source and an optical spectrum analyzer were used as the source and detector for approximate alignment. High spectral resolution results were then obtained by employing a tunable laser (with 10 pm resolution sweep) together with a detector. The average fiber-to-fiber loss was 14 dB, whereas the device insertion loss was 5 dB. Fig. 7(a) shows the reflectivity profile of devices with and without apodization. It is seen that the apodized devices have 1.6-nm (200 GHz) channel spacing with a 0.6-nm (75 GHz) bandwidth. The 0.2-nm reduction in the demonstrated bandwidth compared with that obtained in the simulation is attributed to the reduction in the duty cycle of the gratings during fabrication. The SMSR of the apodized device was 16 dB and that of the unapodized device was 6 dB. The plot also demonstrated the steeper filter rolloff in the dual apodized design. Fig. 7(b) compares the reflectivity in two different apodized devices, i.e., the dual apodized design as in Fig. 3(b) and the $L_1$ modulated design as indicated in Fig. 3(d). It is seen that the dual apodized device performs better than the $L_1$ modulated design in terms of having a wider 3-dB bandwidth and a steeper rolloff; although, the $L_1$ modulated devices have a slightly larger rejection ratio. The difference in the insertion loss between the dual apodized and the $L_1$ modulated schemes is between 2–3 dB over the five channels indicated in Fig. 7(b). This arises due to slight variations in fabrication conditions since the dual apodized and the $L_1$ modulated devices are in different locations within the die.

## 4. Conclusion

In this article, comb filters in SOI based on side-etched sampled gratings have been designed and experimentally demonstrated. We proposed the concept of dual complementary tapering of the marks and spaces to realize a near-zero index change required for obtaining sidelobe-free spectra. We also presented, through numerical modeling, comb filters with a 40-dB side-mode suppression ratio, a 92-GHz clear bandwidth, 200- and 100-GHz channel spacing, and a 120-dB/dec rolloff. When compared with vertically etched gratings, side-etched gratings have the advantage of simple control of the grating depth and a single etch step to fabricate waveguides and gratings. These devices were fabricated in SOI using e-beam lithography and ICP etching. The apodized devices exhibited 200-GHz comb spacing, a 75-GHz 3-dB bandwidth, a 16-dB SMSR, and a filter rolloff of approximately 90 dB/dec. These comb filters demonstrate the potential to be integrated into switches and tunable filters. Future work includes the fabrication of tunable filters using Vernier effect by employing two back-to-back comb cavities with different $L_2/L_1$ ratios and investigating the effect of fabrication errors on filter performance.

## References


[1] A. Misawa, K. Sasayama, and Y. Yamada, "WDM knockout switch with multi-output-port wavelength-channel selectors," *J. Lightw. Technol.*, vol. 16, no. 12, pp. 2212–2219, Dec. 1998.

[2] M. Menard and A. G. Kirk, "Integrated Fabry–Perot comb filters for optical space switching," *J. Lightw. Technol.*, vol. 28, no. 5, pp. 768–775, Mar. 2010.

[3] B. G. Lee, A. Biberman, M. Lipson, and K. Bergman, "All-optical comb switch for multiwavelength message routing in silicon photonic networks," *IEEE Photon. Technol. Lett.*, vol. 20, no. 10, pp. 767–769, May 2008.

[4] M. A. Foster, J. S. Levy, O. Kuzucu, K. Saha, M. Lipson, and A. L. Gaeta, "Silicon-based monolithic optical frequency comb source," *Opt. Exp.*, vol. 19, no. 15, pp. 14 233–14 239, Jul. 2011.

[5] P. Del'Haye, A. Schliesser, O. Arcizet, T. Wilken, R. Holzwarth, and T. J. Kippenberg, "Optical frequency comb generation from a monolithic microresonator," *Nature*, vol. 450, pp. 1214–1217, Dec. 2007.

[6] A. Foltynowicz, P. Masłowski, T. Ban, F. Adler, K. C. Cossel, T. C. Briles, and J. Ye, "Optical frequency comb spectroscopy," *Faraday Discuss.*, vol. 150, pp. 23–31, 2011.

[7] R. Todt, T. Jacke, R. Meyer, R. Laroy, G. Morthier, and M.-C. Amann, "Widely tunable twin-guide laser diodes with sampled gratings: Design and performance," *IEEE J. Sel. Topics Quantum Electron.*, vol. 13, no. 5, pp. 1095–1103, Sep./Oct. 2007.

[8] T. Erdogan, "Fiber grating spectra," *J. Lightw. Technol.*, vol. 15, no. 8, pp. 1277–1294, Aug. 1997.

[9] T. Segawa, S. Matsuo, Y. Ohiso, T. Ishii, and H. Suzuki, "Apodised sampled grating using InGaAsP/InP deep-ridge waveguide with vertical-groove surface grating," *Electron. Lett.*, vol. 40, no. 13, pp. 804–805, Jun. 2004.

[10] D. T. H. Tan, K. Ikeda, and Y. Fainman, "Coupled chirped vertical gratings for on-chip group velocity dispersion engineering," *Appl. Phys. Lett.*, vol. 95, no. 14, pp. 141109-1–141109-3, Oct. 2009.

[11] H.-C. Kim, K. Ikeda, and Y. Fainman, "Resonant waveguide device with vertical gratings," *Opt. Lett.*, vol. 32, no. 5, pp. 539–541, Mar. 2007.

[12] J. T. Hastings, M. H. Lim, J. G. Goodberlet, and H. I. Smith, "Optical waveguides with apodized sidewall gratings via spatial-phase-locked electron-beam lithography," *J. Vac. Sci. Technol. B, Microelectron. Nanometer Struct.*, vol. 20, no. 6, pp. 2753–2757, Nov. 2002.

[13] A. K. Dutta, N. K. Dutta, and M. Fujiwara, *WDM technologies: Active Optical Components*. New York: Academic, 2002.

[14] V. Jayaraman, Z.-M. Chuang, and L. A. Coldren, "Theory, design, and performance of extended tuning range semiconductor lasers with sampled gratings," *IEEE J. Quantum Electron.*, vol. 29, no. 6, pp. 1824–1834, Jun. 1993.

[15] A. Yariv and P. Yeh, *Photonics: Optical Electronics in Modern Communications*. New York: Oxford Univ. Press, 2007.

[16] Y. Shibata, T. Tamamura, S. Oku, and Y. Kondo, "Coupling coefficient modulation of waveguide grating using sampled grating," *IEEE J. Quantum Electron.*, vol. 6, no. 10, pp. 1222–1224, Oct. 1994.

[17] P. S. Cross and H. Kogelnik, "Sidelobe suppression in corrugated-waveguide filters," *Opt. Lett.*, vol. 1, no. 1, pp. 43–45, Jul. 1977.

[18] V. Mizrahi and J. E. Sipe, "Optical properties of photosensitive fiber phase gratings," *J. Lightw. Technol.*, vol. 11, no. 10, pp. 1513–1517, Oct. 1993.

[19] J. E. Sipe, L. Poladian, and C. M. de Sterke, "Propagation through nonuniform grating structures," *J. Opt. Soc. Amer. A*, vol. 11, no. 4, pp. 1307–1320, Apr. 1994.

[20] M. J. Strain and M. Sorel, "Design and fabrication of integrated chirped Bragg gratings for on-chip dispersion control," *IEEE J. Quantum Electron.*, vol. 46, no. 5, pp. 774–782, May 2010.

[21] R. Soref and B. Bennett, "Electrooptical effects in silicon," *IEEE J. Quantum Electron.*, vol. 23, pp. 123–129, 1987.

[22] P. Dong *et al.*, "All-optical compact silicon comb switch," *Opt. Exp.*, vol. 15, no. 1, pp. 9600–9605, Jan. 2007.

[23] G. T. Reed and C. E. Jason Png, "Silicon optical modulators," *Mater. Today*, vol. 8, no. 1, pp. 40–50, 2005.